

# Multi-timescale synaptic plasticity on analog neuromorphic hardware

Amani Atoui<sup>‡,†</sup>, Jakob Kaiser<sup>\*</sup>, Sebastian Billaudelle<sup>†,\*</sup>, Philipp Spilger<sup>\*</sup>, Eric Müller<sup>\*</sup>,  
Jannik Luboeinski<sup>§</sup>, Christian Tetzlaff<sup>§</sup> and Johannes Schemmel<sup>\*</sup>

<sup>\*</sup>*Kirchhoff Institute for Physics, Heidelberg University, Germany*

<sup>†</sup>*Institute for Neuroinformatics, University of Zurich and ETH Zürich, Zürich, Switzerland*

<sup>§</sup>*Group of Computational Synaptic Physiology, Department of Neuro- and Sensory Physiology,  
University Medical Center Göttingen, Germany*

<sup>‡</sup>amani.atoui@kip.uni-heidelberg.de

**Abstract**—As numerical simulations grow in complexity, their demands on computing time and energy increase. Accelerators for numerical computation offer significant efficiency gains in many computationally-intensive scientific fields, but their use in simulating spiking neural networks in computational neuroscience is hindered by challenges, mainly in effective parallelism and efficient use of memory in the presence of sparse representations and sparse communication. The BrainScaleS architectures are neuromorphic substrates that can emulate spiking neural networks at accelerated timescales compared to real time, which offers an advantage for studying complex plasticity rules that require extended simulation runtimes. This work presents the implementation of a calcium-based plasticity rule that integrates calcium dynamics based on the synaptic tagging-and-capture hypothesis on the BrainScaleS-2 system. The implementation of the plasticity rule for a single synapse involves incorporating the calcium dynamics and the plasticity rule equations. The calcium dynamics are mapped to the analog circuits of BrainScaleS-2, while the plasticity rule equations are numerically solved on its embedded digital processors. The main hardware constraints include the speed of the processors and the use of integer arithmetic. By adjusting the timestep of the numerical solver and introducing stochastic rounding, we demonstrate that BrainScaleS-2 accurately emulates a single synapse following a calcium-based plasticity rule across four established stimulation protocols and validate our implementation against a software reference model.

**Index Terms**—neuromorphic, synaptic plasticity, stochastic rounding, memory consolidation

## I. INTRODUCTION

Computer simulations are an indispensable part of computational neuroscience, specifically for understanding neuron circuits through synaptic plasticity [1]. The challenge lies in simulating complex models and large networks with an adequate simulation timestep for the numerical solver to capture milliseconds neuronal activity. This can result in long waiting times when simulating long-term synaptic plasticity which operates in the timescale of several hours [1]. There comes the role of specialized neuromorphic hardware, such as BrainScaleS-2 (BSS-2), that can emulate neural dynamics at accelerated timescales compared to real time.

Our aim is to employ the advantages of neuromorphic hardware for the understanding of synaptic plasticity through calcium-based models. Molecular studies have identified cal-

cium as a key element of plasticity mechanisms, which has motivated its integration into mechanistic models of long-term synaptic plasticity [2], [3]. Such models can describe a diversity of plasticity curves that have been observed experimentally in different systems [2], [4], as well as provide insights into memory consolidation in recurrent neural networks [5].

The synaptic tagging-and-capture (STC) hypothesis provides an explanation of the neuronal and synaptic processes underlying memory consolidation based on evidence from molecular studies [6], [7], [8]. This hypothesis has also been linked to so-called behavioral tagging experiments [9], [10], relating the STC hypothesis to the study of learning and memory in cognitive neuroscience. Theoretical studies of single synapses [11], feedforward neural networks [12], and recurrent neural networks [13] have supported the STC hypothesis and its role in memory consolidation (see [5] for a review).

In this work, we implement a plasticity rule that obeys the STC hypothesis for a single synapse on neuromorphic hardware. Based on this, our end goal is to provide an accelerated implementation of spiking neural networks whose plasticity rule follows the STC hypothesis to answer scientific questions about learning and memory. We start by giving an overview of the BSS-2 system and the plasticity model [13] that we adopt. We also describe useful concepts for our implementation such as the stochastic rounding (SR) scheme. We then list the hardware constraints that we encounter in the implementation and our propositions to overcome them. Our key contributions include updating different model variables on multiple timescales and using SR for integer arithmetic. The results show that the considered plasticity rule can be successfully emulated for a single synapse on BSS-2 due to the compensation across the effects that arise from analog computing and stochasticity across spike trials.

### A. The BrainScaleS-2 System

On the neuromorphic BSS-2 system, neuron and synapse dynamics are emulated by analog circuits. The 512 neuron circuits on the system replicate the behavior of the adaptive exponential leaky integrate-and-fire (AdEx) neuron model [14] in continuous time. BSS-2 emulates these dynamics at a tunable

acceleration factor of 1000 compared to biological real time [15]. The AdEx model consists of two coupled differential equations for the membrane potential  $V(t)$  and the adaptation current  $I_{\text{adapt}}(t)$ . The membrane potential is given by

$$C_m \frac{dV(t)}{dt} = g_L \cdot (V_L - V(t)) + g_L \Delta_T \exp\left(\frac{V(t) - V_T}{\Delta_T}\right) + I_{\text{syn}}(t) - I_{\text{adapt}}(t), \quad (1)$$

where  $C_m$  is the membrane capacitance,  $g_L$  the leak conductance,  $V_L$  the leak potential,  $\Delta_T$  the threshold slope factor and  $V_T$  the effective threshold potential.

The second equation describes the dynamics of the adaptation current

$$\tau_{\text{adapt}} \frac{dI_{\text{adapt}}(t)}{dt} = a (V_m(t) - V_L) - I_{\text{adapt}}(t), \quad (2)$$

where  $\tau_{\text{adapt}}$  is the adaptation time constant and  $a$  the subthreshold adaptation.

$I_{\text{syn}}(t)$  represents the synaptic input current. BSS-2 supports conductance- as well as current-based synapses [15]. In the presented work, we will use current-based synapses, which implement an exponentially decaying current for each input spike, as in [13].

Once the membrane potential  $V$  reaches a threshold potential  $V_{\text{th}}$  the membrane potential is clamped to the reset potential  $V_{\text{reset}}$  for the duration of the refractory period  $\tau_{\text{ref}}$  and the adaptation current  $I_{\text{adapt}}$  is increased by the spike-triggered adaptation  $b$ :  $I_{\text{adapt}} \rightarrow I_{\text{adapt}} + b$ . Furthermore, a digital spike event is generated and forwarded to postsynaptic partners. Each neuron circuit is connected to 256 synapse circuits storing 6 bit weights which convert the digital, presynaptic events to voltage pulses which control the synaptic current on each membrane. Neurons can also be configured such that each presynaptic spike causes a postsynaptic spike, the so-called ‘‘bypass’’ mode.

The modular design of the neuron circuits allows to selectively enable and disable features of the neuron. For example, the exponential and adaptation terms can be disabled to reduce the neuron model to a leaky integrate-and-fire (LIF) neuron model. In addition, an analog dynamic memory array [16] allows to adjust each of the parameters mentioned in eqs. (1) and (2) individually for each neuron.

The BSS-2 application-specific integrated circuit (ASIC) is organized in two halves with 256 neurons at the top and 256 neurons at the bottom, see fig. 1. Each half of the chip also hosts a digital processor. These so-called plasticity processing units (PPUs) implement the Power instruction set architecture (ISA) 2.06 [17] for 32 bit and a custom vector unit extension. The PPU can access a vector-parallel columnar analog-to-digital converter (CADC), which enables to sample, for example, the adaptation currents of several neurons in parallel. Furthermore, it can modify the neuron parameters as well as the synaptic weights [18]. While the PPU does not provide direct access to spikes and membrane analog-to-digital converter (MADC) data, the data can in principle be recorded to field-programmable gate

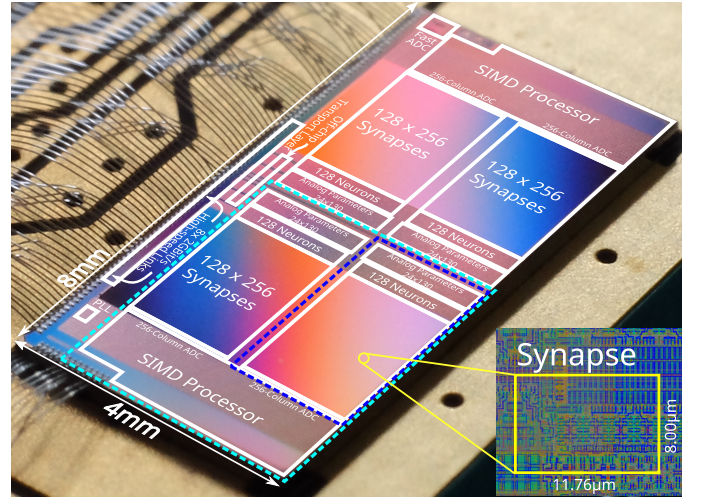


Figure 1. Schematic and chip photo of the BSS-2 application-specific integrated circuit (ASIC). One embedded SIMD processor per chip half can run arbitrary code to access on-chip observables, such as membrane potentials, and to perform changes to topology, neuron and synapse parameterization.

array (FPGA)-based dynamic random-access memory (DRAM) which is accessible to the embedded processors and the host computer.

The BSS-2 software stack provides a high-level modeling interface for experiment definition and a C++ [19] runtime with a focus on embedded real-time programming to express programmable processes and plasticity rules on the PPU.

### B. Memory and Synaptic Tagging-and-Capture Hypothesis

An important physical substrate for the emergence of long-term memory (LTM) is the stabilization of synaptic efficacies within neural networks, referred to as synaptic consolidation. The biological mechanisms proposed to underlie synaptic consolidation involve two different phases [6], [20], [21]: the early phase is characterized by receptor alterations and turnover based on the calcium concentration in the postsynapse, while the late phase is characterized by the addition of receptor slots in the case of potentiation and their removal in the case of depression. The transfer from the early-phase to the late-phase is achieved by biophysical and structural alterations in the synapses that contribute to stabilizing the levels of synaptic strength.

The STC hypothesis [6], [8] is a specific theory that has been found to explain main aspects of synaptic consolidation [5], [20], [21]. It adopts the concept that early-phase plasticity creates a potential for stable synaptic weight changes while not being stable itself [6], [13]. According to the STC hypothesis, late-phase plasticity occurs after neurons have fired sufficiently. It consists of the following steps. First, early-phase plasticity is expressed, and the synapse is marked with a local synaptic tag for specificity. Second, proteins are synthesized and distributed. Third, these proteins are captured by the tagged synapses which allow the stabilization of the synaptic strength in the late phase.

The time course of synaptic consolidation is influenced by the recent history and near future of the network activity [6],

[8], thus, it involves a set of mechanisms that can but do not have to be triggered at a single moment in time. Through the interaction of the network with the synthesized proteins and synaptic tags, the STC hypothesis accounts for the time window of initial (synaptic) memory consolidation.

### C. Plasticity Equations

We use the synapse model from [13] that integrates the calcium dynamics with the STC hypothesis. The neuron dynamics follow the LIF model. For our work, we consider a single synapse between a presynaptic neuron  $j$  and a postsynaptic neuron  $i$ . The calcium dynamics of the postsynaptic site are given by

$$\begin{aligned} \frac{dc(t)}{dt} = & -\frac{c(t)}{\tau_c} + c_{\text{pre}} \sum_n \delta(t - t_j^n - t_{c,\text{delay}}) \\ & + c_{\text{post}} \sum_m \delta(t - t_i^m), \end{aligned} \quad (3)$$

with the calcium time constant  $\tau_c$ , the presynaptic spike times  $t_j^n$ , the postsynaptic spike times  $t_i^m$ , the contribution of presynaptic spikes  $c_{\text{pre}}$ , the contribution of postsynaptic spikes  $c_{\text{post}}$ , and the delay of calcium concentration triggered by presynaptic spikes  $t_{c,\text{delay}}$ .

The dynamics of the early-phase weight  $h(t)$  of the synapse (given in units of nanocoulomb) are governed by

$$\begin{aligned} \tau_h \frac{dh(t)}{dt} = & 0.1 (h_0 - h(t)) \\ & + \gamma_p (h_{\text{max}} - h(t)) \cdot \Theta[c(t) - \theta_p] \\ & - \gamma_d (h(t) - h_{\text{min}}) \cdot \Theta[c(t) - \theta_d] + \xi(t), \end{aligned} \quad (4)$$

with  $\Theta[\cdot]$  being the Heaviside function and  $\tau_h$  being a time constant. The first term of eq. (4) describes a relaxation of the early-phase weight to its initial value  $h_0$ , the second term describes early-phase long-term potentiation (LTP) with a rate  $\gamma_p$  for calcium concentration above the potentiation threshold  $\theta_p$ , and the third term describes early-phase long-term depression (LTD) with a rate  $\gamma_d$  for calcium concentration above the depression threshold  $\theta_d$ . The term  $\xi(t)$  describes the calcium-dependent noise-driven fluctuations. The weight dynamics are bounded by  $h_{\text{max}} = 1 \text{ nC}$  and  $h_{\text{min}} = 0 \text{ nC}$ .

The protein amount  $p(t)$  for the postsynaptic neuron is updated using

$$\tau_p \frac{dp(t)}{dt} = -p(t) + \alpha \Theta[|h(t) - h_0| - \theta_{\text{pro}}], \quad (5)$$

where  $\alpha$  is the protein synthesis rate and  $\theta_{\text{pro}}$  is the protein synthesis threshold.

The dynamics of the late-phase weight  $z(t)$  of the synapse depend on the protein amount  $p(t)$ , early-phase weight  $h(t)$ , and a tagging threshold  $\theta_{\text{tag}}$  as

$$\begin{aligned} \tau_z \frac{dz(t)}{dt} = & p(t) \cdot (z_{\text{max}} - z(t)) \cdot \Theta[(h(t) - h_0) - \theta_{\text{tag}}] \\ & - p(t) \cdot (z(t) - z_{\text{min}}) \cdot \Theta[(h_0 - h(t)) - \theta_{\text{tag}}]. \end{aligned} \quad (6)$$

The late-phase weight is bounded by  $z_{\text{max}} = 1$  and  $z_{\text{min}} = -0.5$ . Finally, the total synaptic weight  $w(t)$  is given by

$$w(t) = h(t) + h_0 \cdot z(t). \quad (7)$$

### D. Integer Arithmetic

The PPU does not feature hardware support for floating-point arithmetic [22]. Instead, numeric calculations have to be implemented using 8 bit and 16 bit integers. This means that variables are represented using a maximum dynamic range of  $[0 \dots \text{MAX\_UINT}_n = 2^n - 1]$  for unsigned  $n$ -bit integers and  $[\text{MIN\_INT}_n = -2^{n-1} \dots \text{MAX\_INT}_n = 2^{n-1} - 1]$  for signed  $n$ -bit integers. This reduced arithmetic is advantageous in terms of silicon space, energy, and memory storage, but it also imposes challenges in terms of resolution and truncation [23]. By default, operations on integers implement the *truncate-to-zero* mode, which becomes problematic when adding fractional amounts or dividing by integers; this mode typically accumulates errors and produces underestimated final results.

Other challenges can be a consequence of the programming language. Because C and C++ focus on processing speed, they open up many possibilities for triggering undefined behavior when performing integer arithmetic operations [24], [25].

To overcome the numerical errors from using integer arithmetic, the stochastic rounding mode was suggested in [26]. In the SR mode, a given number is mapped to one of the two nearest representable numbers with a probability that depends on the distances of the given number to the nearest numbers.

There are two main situations where SR is useful. First, SR ensures zero-mean rounding errors and produces smaller errors especially in situations where *truncate-to-zero* produces rounding errors of one sign [27]. Suppose an integer  $x$  is multiplied with a fraction  $\frac{n}{d}$ . The result with *truncate-to-zero* is an integer  $y$  such that

$$y = \lfloor x \cdot \frac{n}{d} \rfloor, \quad (8)$$

which accumulates an error

$$\epsilon = \frac{(x \cdot n) \bmod d}{d}. \quad (9)$$

This can be overcome by stochastically compensating for the error

$$y' = \begin{cases} \lceil x \cdot \frac{n}{d} \rceil = y + 1 & \text{with probability } \epsilon, \\ \lfloor x \cdot \frac{n}{d} \rfloor = y & \text{with probability } 1 - \epsilon. \end{cases} \quad (10)$$

Second, SR is immune to stagnation, a phenomenon where a sequence of small updates relative to large quantities is lost if these changes cannot be represented by the machine's number format. Suppose an integer  $x$  is successively updated by a fixed amount  $\epsilon < 1$  such that

$$x' = x + \epsilon. \quad (11)$$

Since  $\epsilon$  cannot be represented by an integer, SR proposes updating  $x$  according to

$$x' = \begin{cases} x + 1 & \text{with probability } \epsilon, \\ x & \text{with probability } 1 - \epsilon. \end{cases} \quad (12)$$

While SR has been known since the 1950s, the interest in it is currently expanding as it proved useful in applications mainly

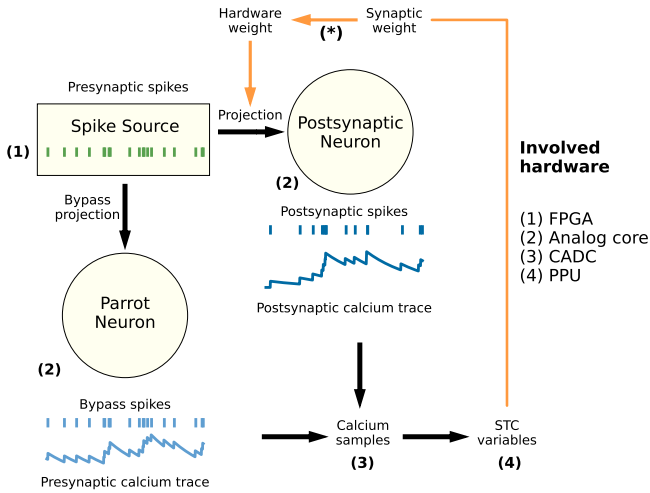


Figure 2. Experimental setup for emulating a single synapse following the considered plasticity rule on BSS-2. The FPGA provides a real-time capable memory-buffered input and output interface for the neuromorphic chip. A spike source is placed on the FPGA and used to generate presynaptic spikes. These are forwarded to the postsynaptic neuron via a projection whose weight update obeys the considered plasticity rule. The same presynaptic spikes are mirrored to the parrot neuron to emulate the presynaptic calcium dynamics. The “bypass” mode of the parrot neuron ensures that presynaptic spikes are immediately translated to postsynaptic spikes. The weighted sum of the adaptation traces of the postsynaptic and parrot neurons represents the calcium trace. Calcium samples obtained by the CADC are then used by the PPU to calculate the model variables, including the synaptic weight, which will be used to update the weight of the projection. The mapping of the synaptic weight to hardware indicated by (\*) has a negligible effect in the considered single synapse case, so we chose not to implement it in this work.

related to machine learning and solving ordinary differential equations on reduced precision systems. SR was proposed to overcome the resulting numerical drawbacks and was proven useful in different use cases such as solving ordinary differential equations to produce accurate spike timings in the Izhikevich neuron model [23].

## II. METHODS

In this work, we exploit the concept of updates at different timesteps. Unlike numerical simulations on conventional hardware, which typically define a unified timestep to update all the model variables, we use different timesteps depending on the involved hardware and time constants. This is done since part of the variables are emulated in continuous time in the analog core of BSS-2 while others are solved numerically on an embedded processor. Specifically, the membrane potential and calcium concentration will be emulated as continuous-time analog signals, the transient early-phase weight will be updated regularly, and the early-phase weight relaxation, late-phase weight, and protein amount will be updated stochastically.

### A. Experimental Setup on BrainScaleS-2

The experimental setup for the emulation of the plasticity rule is shown in fig. 2. Here, we explain the intuition behind our approach and discuss the details of the involved hardware.

The neuron dynamics are emulated by the analog core of BSS-2 while the synaptic weights can be computed numerically on a fixed time grid using the PPU. An important consideration here is to link the fast timescale of the neuron dynamics and spikes to the slow timescale of the synaptic weight dynamics. This link is achieved by the calcium concentration that directly depends on the spikes, but also drives the updates of the synaptic weights. Therefore, we map the calcium concentration to the analog circuit using the adaptation current (eq. (2)) whose dynamics greatly resemble those of the calcium concentration (eq. (3)). The calcium traces are then sampled from the analog core at a fixed sampling period  $\Delta t$ , and these samples are used to update the synaptic weights. In this way, the calcium concentration acts as a domain crossing that maps the fast neuron dynamics to the slow synaptic weight dynamics.

To set up the experiment on BSS-2, a spike source is configured that plays the role of the presynaptic neuron which injects spikes into a postsynaptic neuron. For the considered plasticity rule, additional requirements apply. The adaptation trace generated by the postsynaptic neuron depends on the postsynaptic spikes only, but the calcium trace depends on the presynaptic and postsynaptic spikes. To track the contribution of presynaptic spikes, we exploit the linearity of eq. (3) which allows us to split the equation into a presynaptic component and a post-synaptic component. We use an additional neuron, called “parrot neuron”, to account for the contribution of the presynaptic spikes. This circuit is connected to the same spike source and is configured in the “bypass” mode such that every input spike triggers an output spike. In this way, we mirror the presynaptic spikes and obtain an adaptation trace from the spikes of the parrot neuron. The required calcium trace is thus the weighted sum of the two adaptation traces.

Simulation results showed that the calcium contribution of postsynaptic spikes is negligible compared to that of the presynaptic spikes in the given stimulation protocols. Thus, the main focus of this work is the implementation of the calcium dynamics in general as well as the plasticity equations. The synaptic weight is not mapped to hardware, but is set to a small value such that no post-synaptic spikes occur.

### B. Stimulation Protocols

To model the different forms of plasticity that could occur in a single synapse, we use the standard stimulation protocols that are generally adopted in the literature (provided in the supplementary information of [13]). Tetanic (high-frequency) stimulations induce LTP due to the high calcium concentration released at the synapse while low-frequency stimulations induce LTD due to the moderate calcium concentration. Furthermore, strong stimulations cause the synapse to be marked by a local synaptic tag and the synthesis of a sufficient amount of plasticity-related proteins (PRPs) necessary for late-phase synaptic plasticity whereas weak stimulations only induce synaptic tagging and early-phase plasticity. Consequently, the strong tetanic stimulation (STET) protocol induces early-phase and late-phase LTP whereas weak tetanic stimulation (WTET) protocol induces only early-phase LTP. On the other hand, the

strong low-frequency stimulation (SLFS) protocol induces early-phase and late-phase LTD whereas the weak low-frequency stimulation (WLFS) protocol induces only early-phase LTD.

### C. Hardware Constraints and Limitations

Using BSS-2 for implementing the plasticity rule imposes constraints that we should resolve:

- 1) Plasticity rule timestep: this timestep accounts for the time required by the PPU to sample from the analog traces and compute the weight update. The timestep of the numerical solver used in the model simulation in [13] was 0.2 ms which is equivalent to 0.2  $\mu$ s in our experiment parameterization on BSS-2. This interval is too short for the current implementation on the PPU, so we aimed to use slower updates. On the other hand, performing the numerical integration of the plasticity equations at long timesteps does not capture the required dynamics and yields distorted results. To ensure the expected behavior of the stimulation protocols in terms of early and late LTP and LTD, we found that this timestep must not exceed 100  $\mu$ s and preferably remain below 50  $\mu$ s.
- 2) Integer arithmetic: The simulations in [13] were performed using double-precision floating-point arithmetic, which is not supported by the PPU. While floating-point numerics can be simulated in software, we prioritize using native integer arithmetic for speed purposes. Specifically, we use 8 bit integers for representing the model variables, and 32 bit integer arithmetic for operations and random number generation. This necessitates converting the model variables to a suitable dynamic range and further approximating model parameters, but also imposes truncation errors.
- 3) Large time constants: these lead to slow changes of the model variables such as the protein amount, the late-phase weight, and the steady-state term of the early-phase weight. This leads to stagnation since the changes in the state variables and synaptic weights are small and cannot be represented by 8 bit integers. To resolve this, we suggest using a stochastic-update method.

Besides these constraints, there remain distortions that are not resolved for the current emulation of the neuron and calcium dynamics:

- 1) The postsynaptic calcium influx delay arising from the presynaptic spikes, described in eq. (3) as  $t_{c,delay}$  will not be implemented. The reason is that the calcium traces are generated by the adaptation traces whose circuits are designed to increment the adaptation term at the spike time with no possibility for a predefined delay.
- 2) The axonal spike delay will not be implemented as the circuits for emulating neuron dynamics do not account for this delay.
- 3) The noise fluctuations of calcium during potentiation and depression that affect the early-phase weight, referred to as  $\xi(t)$  described in eq. (4), will not be applied since it is computationally expensive.

As we will show below, however, these limitations do not substantially affect our emulation of early- and late-phase synaptic plasticity dynamics on BSS-2.

### D. Mapping Calcium to Adaptation Current

As mentioned earlier, we split the calcium concentration into pre- and postsynaptic components and use the adaptation term to emulate the two components. What makes the use of the adaptation term possible is that it can be enabled without affecting the neuron dynamics. For each component, we set the subthreshold adaptation strength  $a = 0$  since the calcium concentration does not depend on the membrane potential. The time constant  $\tau_{adapt}$  is mapped to the calcium time constant  $\tau_c$ . The spike-triggered increment  $b$  should be mapped to the contributions of presynaptic and postsynaptic spikes  $c_{pre}$  and  $c_{post}$ . An important consideration is that  $b$  should also be tuned to ensure a high dynamic range with a linear behavior of the circuit.

For tuning the adaptation parameters and comparing against the biological calcium trace in eq. (3), we rely on the membrane analog-to-digital converter (MADC). Although the MADC will not be used for sampling the calcium traces when running the plasticity rule on BSS-2, it has a higher sampling rate and a finer resolution compared to the CADC. Therefore, the adaptation traces can be retrieved, and the parameters can be fine-tuned to match the theoretical calcium trace. We use the experimental setup described in fig. 2 and a stimulation scheme of Poisson spikes at 100 kHz for the tuning. While running the plasticity rule, the calcium traces will be sampled using the CADC at a lower sampling rate.

### E. Mapping Biological Parameters to Hardware

For the emulation on BSS-2, we map all parameters in the plasticity equations to hardware. Parameters concerned with time dynamics such as  $\tau_h$ ,  $\tau_p$ ,  $\tau_z$ , and  $\tau_c$  are divided by the acceleration factor of 1000, while multiplicative factors such as  $\gamma_p$  and  $\gamma_d$  are kept constant. As mentioned previously, the model variables are represented using integer arithmetic. Specifically, the early-phase weight  $h$  and protein amount  $p$  are represented using unsigned 8 bit integers, while the late-phase weight  $z$  is represented using a signed 8 bit integer. The initial or steady-state values  $h_0 = 0.420\,075$  nC,  $h_{max} = 1$  nC,  $h_{min} = 0$  nC,  $z_{min} = -0.5$ , and  $z_{max} = 1$  are mapped to the ranges of their corresponding variables. This yields  $h_0^{hw} = \lfloor h_0 \cdot \text{MAX\_UINT}_8 \rfloor$ ,  $h_{max}^{hw} = \text{MAX\_UINT}_8$ ,  $h_{min}^{hw} = \text{MIN\_UINT}_8$ ,  $z_{min} = 0.5 \cdot \text{MIN\_INT}_8$ , and  $z_{max} = \text{MAX\_UINT}_8$ . Similarly, the protein and tagging thresholds  $\theta_{pro}$  and  $\theta_{tag}$  are mapped to the range of  $h$ . Since we tune the calcium dynamics on the adaptation circuit, the calcium thresholds  $\theta_p$  and  $\theta_d$  are mapped experimentally using linear regression.

### F. Solving the Differential Equations

To solve the differential equations of  $h$ ,  $p$ , and  $z$  in the plasticity kernel, we use the explicit Euler method. For a first-

order differential equation  $\frac{dy(t)}{dt} = F(t, y)$  and regular time step  $\Delta t$ , we can write the explicit Euler formula as

$$y(t_n + \Delta t) = y(t_n) + \Delta t \cdot F(t_n, y(t_n)). \quad (13)$$

To overcome the numerical errors from *truncate-to-zero* in solving the differential equations, we apply SR. We use random 32 bit unsigned integers drawn from a 32 bit xorshift pseudo-random number generator (PRNG) [28]. The probabilities are then converted to integers by multiplying each probability with  $\text{MAX\_UINT}_{32}$  at runtime to obtain *probability-equivalents*, and the 32 bit random numbers are compared against these probability-equivalents.

1) *Early-phase weight*: Using eq. (13), the differential equation for the early-phase weight  $h$  in eq. (4) can be rewritten as

$$\begin{aligned} h(t + \Delta t) = & h(t) + \frac{0.1 \cdot \Delta t}{\tau_h} (h_0 - h(t)) \\ & + \frac{\gamma_p \cdot \Delta t}{\tau_h} \cdot (255 - h(t)) \cdot \Theta[c(t) - \theta_p] \\ & - \frac{\gamma_d \cdot \Delta t}{\tau_h} \cdot h(t) \cdot \Theta[c(t) - \theta_d]. \end{aligned} \quad (14)$$

The early-phase weight dynamics allows us to divide the equation into three parts. The first two parts are related to plasticity in the presence of sufficient calcium while the third part always pull the early-phase weight to a steady-state value.

1) Plasticity cases:

Case of LTP:  $c \geq \theta_p > \theta_d$  yields

$$h(t + \Delta t) = h(t) \cdot \left(1 - \frac{\Delta t}{\tau_h} \cdot (\gamma_p + \gamma_d)\right) + \frac{\gamma_p \cdot \Delta t \cdot 255}{\tau_h}, \quad (15)$$

Case of LTD:  $\theta_p > c \geq \theta_d$  yields

$$h(t + \Delta t) = h(t) \cdot \left(1 - \frac{\gamma_d \cdot \Delta t}{\tau_h}\right). \quad (16)$$

Since we multiply the early-phase weight with fractions  $\frac{n}{d}$  for the two plasticity cases, we apply SR, eq. (10), to the final value of  $h$  as

$$h(t + \Delta t) = \begin{cases} h(t + \Delta t) + 1 & \text{if } P_h \leq \theta_h, \\ h(t + \Delta t) & \text{if } P_h > \theta_h, \end{cases} \quad (17)$$

where  $\theta_h = \text{MAX\_UINT}_{32} \cdot \frac{(h(t) \cdot n) \bmod d}{d}$  and  $P_h$  is a 32 bit random number. In the potentiation case, we have an additional fractional offset, so we also apply SR, eq. (12), to this part.

2) Steady-state: this part of the equation forces  $h$  to converge to a steady-state value  $h_0$  with a time constant of  $10 \cdot \tau_h$

$$h(t + \Delta t) = \begin{cases} h(t) + 1 \cdot \text{sgn}(h_0 - h(t)) & \text{if } P_{h,ss} \leq \theta_{h,ss}, \\ h(t) & \text{if } P_{h,ss} > \theta_{h,ss}, \end{cases} \quad (18)$$

with  $\theta_{h,ss} = \text{MAX\_UINT}_{32} \cdot \frac{0.1 \Delta t \cdot |h_0 - h(t)|}{\tau_h}$  and  $P_{h,ss}$  being a 32 bit random number. We chose  $P_{h,ss}$  to be dependent on  $h_0 - h(t)$  so that  $h(t)$  converges smoothly.

The differential equation for the protein amount  $p$  in eq. (5) can be rewritten as

$$\begin{aligned} p(t + \Delta t) = & p(t) - p(t) \cdot \frac{\Delta t}{\tau_p} \\ & + \frac{\alpha \cdot \Delta t}{\tau_p} \cdot \Theta[|h(t) - h_0| - \theta_{pro}]. \end{aligned} \quad (19)$$

Since  $\frac{\Delta t}{\tau_p} < 1$  and  $\frac{\alpha \cdot \Delta t}{\tau_p} < 1$ , the evolution of the protein dynamics can be expressed as a sum comprising two summands:

1) Case of protein synthesis during late-phase synaptic plasticity:  $|h(t) - h_0| > \theta_{pro}$  yields

$$p(t + \Delta t)_{ps} = \begin{cases} p(t) + 1 & \text{if } P_{p,s} \leq \theta_{p,s}, \\ p(t) & \text{if } P_{p,s} > \theta_{p,s}, \end{cases} \quad (20)$$

with  $\theta_{p,s} = \text{MAX\_UINT}_{32} \cdot \frac{\alpha \cdot \Delta t}{\tau_p}$  and  $P_{p,s}$  a 32 bit random number.

2) Steady-state: this part of the equation allows the protein amount to decay back to 0 which yields

$$p(t + \Delta t)_{ss} = \begin{cases} p(t) - 1 & \text{if } P_{p,ss} \leq \theta_{p,ss}, \\ p(t) & \text{if } P_{p,ss} > \theta_{p,ss}, \end{cases} \quad (21)$$

where  $\theta_{p,ss} = \text{MAX\_UINT}_{32} \cdot p(t) \cdot \frac{\Delta t}{\tau_p}$  and  $P_{p,ss}$  is a 32 bit random number. We chose  $P_{p,ss}$  to be dependent on  $p(t)$  so that  $p(t)$  decays smoothly and more frequently.

Finally, the differential equation for the late-phase weight  $z$  in eq. (6) can be rewritten as

$$\begin{aligned} z(t + \Delta t) = & z(t) \\ & + \frac{p(t) \cdot \Delta t}{255 \cdot \tau_z} \cdot (127 - z(t)) \cdot \Theta[(h(t) - h_0) - \theta_{tag}] \\ & - \frac{p(t) \cdot \Delta t}{255 \cdot \tau_z} \cdot (z(t) + 64) \cdot \Theta[(h_0 - h(t)) - \theta_{tag}]. \end{aligned} \quad (22)$$

The evolution of the late-phase weight dynamics follows two cases:

1) Case of late LTP:  $h(t) - h_0 \geq \theta_{tag}$  yields

$$z(t + \Delta t)_p = \begin{cases} z(t) + 1 & \text{if } P_{z,p} \leq \theta_{z,p}, \\ z(t) & \text{if } P_{z,p} > \theta_{z,p}, \end{cases} \quad (23)$$

where  $\theta_{z,p} = \text{MAX\_UINT}_{32} \cdot \frac{p(t) \cdot \Delta t}{255 \cdot \tau_z} \cdot (127 - z(t))$  and  $P_{z,p}$  is a 32 bit random number.

2) Case of late LTD:  $h_0 - h(t) \geq \theta_{tag}$  yields

$$z(t + \Delta t)_d = \begin{cases} z(t) - 1 & \text{if } P_{z,d} \leq \theta_{z,d}, \\ z(t) & \text{if } P_{z,d} > \theta_{z,d}, \end{cases} \quad (24)$$

where  $\theta_{z,d} = \text{MAX\_UINT}_{32} \cdot \frac{p(t) \cdot \Delta t}{255 \cdot \tau_z} \cdot (z(t) + 64)$  and  $P_{z,d}$  is a 32 bit random number.

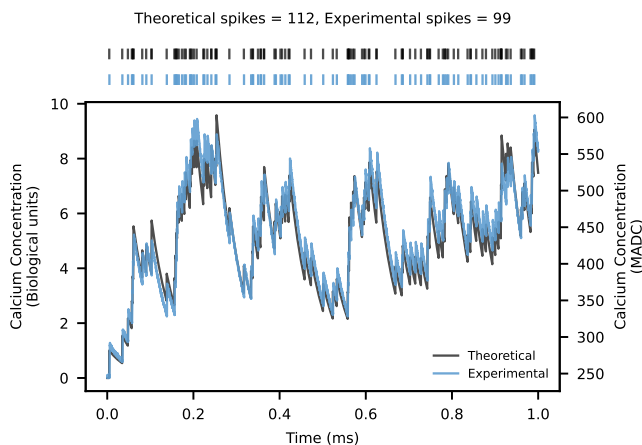


Figure 3. Emulation of calcium dynamics recorded using the MADC at 100 kHz stimulation frequency. The theoretical calcium trace is calculated from Poisson spikes using eq. (3). The experimental calcium trace is extracted using the adaptation trace of the AdEx model from the recorded spikes. The theoretical spikes are Poisson spikes simulated at 100 kHz during 1 ms, and the experimental spikes are recorded from the parrot neuron.

### III. RESULTS

#### A. Emulating the Calcium Dynamics

The parameters of the adaptation signal are tuned to match the biological calcium trace (eq. (3)). Figure 3 shows the results of the tuning for Poisson spikes simulated at a 100 kHz stimulation frequency. Overall, the hardware-emulated calcium trace tracks the numerically computed calcium trace. However, a slight misalignment exists for two reasons. First, the adaptation circuit is non-linear beyond certain adaptation potentials. Second, there is a probability of missing spikes. The misalignment from the nonlinearity of the circuit at high adaptation potentials can be reduced by further tuning specific parameters, specifically by reducing the spike-triggered adaptation  $b$  parameter. This reduces the adaptation potentials and allows the circuit to operate in the linear range at high frequency stimulations. However, this comes with drawbacks at lower stimulation frequencies where the recorded adaptation potentials are not high, and where the depression threshold  $\theta_d^{hw} = b$  can be easily corrupted by noise.

#### B. Running the Plasticity Algorithm

The differential equations are solved with a numerical timestep  $\Delta t = 50 \mu\text{s}$ . First, we run the experiment for 100 different update seeds and a fixed input spike pattern. Due to updating variables at different iterations, each individual update seed yields a different trace but a common overall behavior, fig. 4. Averaging across the update seeds produces a behavior similar to the one obtained from a simulation at a timestep of 50 ms, compare fig. 5.

Second, we run the experiment for 100 spike trials; as in [13], the target is to obtain the average behavior of the synaptic weights to the stimulation protocols across different spike trials. We plot the results against the simulation baseline at a

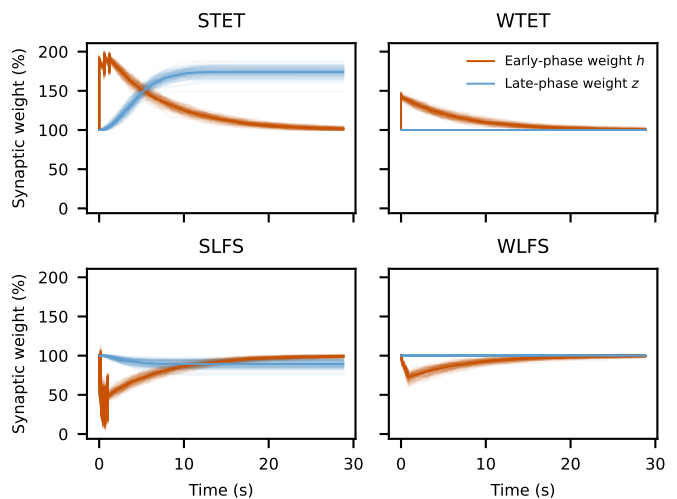


Figure 4. Emulation results for the four stimulation protocols for one spike trial and 100 different update seeds. The trajectories in faded color show the individual trials, and the trajectory in bold shows the average behavior. The overall average behavior is in agreement with the behavior obtained by simulation for the four protocols.

timestep of  $50 \text{ ms}_{\text{bio}}$  in figure 5. For the simulation baseline, we also use the concept of multi-timestep updates where the membrane potential and calcium concentration are updated at a timestep  $0.2 \text{ ms}_{\text{bio}}$  while synaptic weights and protein amount are updated at  $50 \text{ ms}_{\text{bio}}$ .

The mean of the synaptic weights aligns with those obtained from the simulation with small differences. The variances of the emulation are close to the simulation for all protocols except for the STET protocol. This can be attributed to the robustness of the STET protocol and the dominance of the effects that arise from the analog nature of the hardware and stochastic rounding. For the other protocols, the results show that the effects in the hardware variability seem to cancel out with different spike trials.

### IV. DISCUSSION

We implemented and validated a calcium-based plasticity rule integrating the STC hypothesis on BSS-2. Our approach faithfully reproduces the simulation results of the single synapse for four typical stimulation protocols with small differences in the mean and standard deviation. This highlights the power of stochastic rounding for integer arithmetic and reduced precision. The differences between the emulation at a time update of  $50 \mu\text{s}_{\text{hw}} = 50 \text{ ms}_{\text{bio}}$  and the simulation at a time update of 50 ms can be primarily attributed to the variability in the calcium dynamics due to the analog nature of the hardware. The weight update is sensitive to this variability because the calcium dynamics are fast and can decay quickly or rise almost instantaneously by the effect of spikes.

Another important consideration is tuning the parameters of the adaptation circuit that is used to emulate the calcium dynamics. The tuning has to account for circuit linearity and the operation at all considered stimulation frequencies. This presents a challenge since there is a trade-off between the

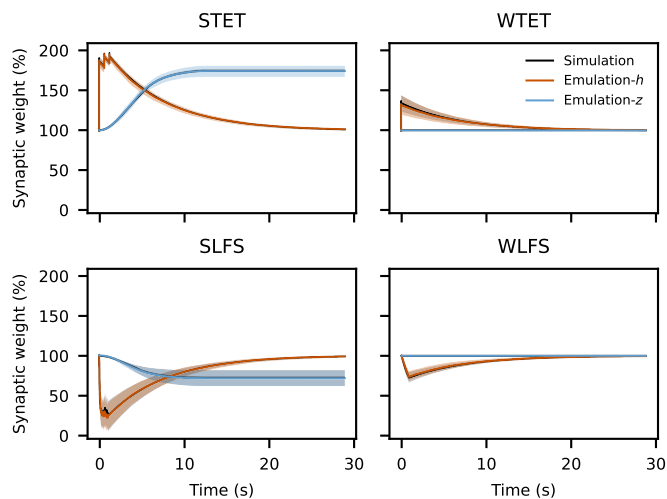


Figure 5. Emulation results for the four stimulation protocols compared against a simulation baseline at a time step of 50 ms for 100 different spike trials. The lines correspond to the average early-phase and late-phase weights. The bands correspond to one standard deviation from the average. For comparison purposes, the simulation results are plotted at an accelerated factor of 1000 to match the time of the emulation results.

tuning at low frequencies and high frequencies. To further improve the results, we may optimize the tuning process of the adaptation parameters using numerical tests and an iterative process.

We consider our implementation of the plasticity rule successful since the overall variability stems from the spike variability, as in the simulation case. In other words, the effects that arise from the analog nature of the hardware and stochastic rounding are compensated across different trials. This is clear from the experiments across different spike trials, where the mean and variance of the synaptic weights in the emulation are almost equal to those of the simulation case in the four stimulation protocols. For the STET protocol, these effects are more apparent, as indicated by the high variance compared to the simulation. The reason is that the STET protocol is considered robust due to its high calcium concentration, making it less prone to the variability in calcium dynamics.

Our work can be expanded to emulate networks on BSS-2 with neurons that follow the investigated plasticity rule, similar to [13]. The network emulation on BSS-2 is made possible through built-in units that undergo parallel computations [29], [30]. We expect that the reduced runtime of the network emulation due to the acceleration factor of BSS-2 allows to run experiments for different network topologies, neuron parametrization, and a higher number of spike trials.

This study showcases that analog neuromorphic hardware can facilitate the investigation of research questions that are unsuitable for numerical simulations due to long simulation runtimes. In principle, accelerated neuromorphic substrates are well-suited for extended-duration experiments, parameter sweeps, or iterative experiment reconfiguration. However, the use of neuromorphic systems comes at a cost: network topologies, model parametrization, and dynamic behavior of neurons

and synapses, as well as plasticity rules must be adapted to the substrate. Especially for neuroscientific research questions, we expect neuromorphic hardware to be complemented by traditional simulation methods. In this complementary approach, the exploration of experiment parametrization, and, in particular, the directed evaluation and reconfiguration of experiments should be offloaded to neuromorphic accelerators, while the simulator provides validation, digital reproducibility, and high numerical precision.

This purpose can be served well by BSS-2, as its integration into the open research infrastructure EBRAINS<sup>1</sup> has enabled the global research community to access the neuromorphic platform.

#### ACKNOWLEDGEMENTS

This work has received funding from the EC Horizon Europe Framework Programme under grant agreement 101147319 (EBRAINS 2.0), the Deutsche Forschungsgemeinschaft (DFG, German Research Foundation) under Germany’s Excellence Strategy EX 2181/1-390900948 (the Heidelberg STRUCTURES Excellence Cluster) as well as through grants SFB1286/C01&Z01, TE 1172/7-1 [CT] and the Bundesministerium für Bildung und Forschung (BMBF), grant number 01IS22093A-E [CT].

#### AUTHOR CONTRIBUTIONS

We give contributions in the *CRedit* (Contributor Roles Taxonomy) format: **AA**: Investigation, visualization, methodology, software; **JK**: Conceptualization, methodology, supervision, software, visualization; **SB**: Conceptualization, methodology, supervision; **PS**: Validation, software, resources; **EM**: Conceptualization, methodology, supervision, software, resources; **JL**: Validation, methodology, software; **CT**: Validation, methodology, funding acquisition; **JS**: Conceptualization, methodology, supervision, funding acquisition; **all**: writing — original draft, writing — reviewing & editing.

#### REFERENCES

- [1] F. Zenke et al., “Limits to high-speed simulations of spiking neural networks using general-purpose computers,” *Front. Neuroinform.*, vol. 8, no. 76, 2014. DOI: 10.3389/fninf.2014.00076
- [2] M. Graupner et al., “Calcium-based plasticity model explains sensitivity of synaptic changes to spike pattern, rate, and dendritic location,” *Proc. Natl. Acad. Sci.*, vol. 109, no. 10, pp. 3991–3996, 2012. DOI: 10.1073/pnas.1109359109
- [3] Y. Li et al., “Induction and consolidation of calcium-based homo- and heterosynaptic potentiation and depression,” *PLoS one*, vol. 11, no. 8, e0161679, 2016. DOI: 10.1371/journal.pone.0161679

<sup>1</sup><https://ebrains.eu>

- [4] S. Sajikumar et al., “Synaptic tagging and cross-tagging: The role of protein kinase m $\zeta$  in maintaining long-term potentiation but not long-term depression,” *Journal of Neuroscience*, vol. 25, no. 24, pp. 5750–5756, 2005. DOI: 10.1523/JNEUROSCI.1104-05.2005
- [5] J. Luboeinski et al., “Modeling emergent dynamics arising from synaptic tagging and capture at the network level,” in *Synaptic Tagging and Capture: From Synapses to Behavior*, S. Sajikumar et al., Eds., 2nd, Cham, Switzerland: Springer, 2024, ch. 23, pp. 471–503. DOI: 10.1007/978-3-031-54864-2\_23
- [6] R. L. Redondo et al., “Making memories last: The synaptic tagging and capture hypothesis,” *Nat Rev Neurosci*, vol. 12, no. 1, pp. 17–30, 2011. DOI: 10.1038/nrn2963
- [7] K. L. Shires et al., “Synaptic tagging and capture in the living rat,” *Nature Communications*, vol. 3, no. 1, p. 1246, 2012. DOI: 10.1038/ncomms2250
- [8] U. Frey et al., “Synaptic tagging and long-term potentiation,” *Nature*, vol. 385, no. 6616, pp. 533–536, 1997. DOI: 10.1038/385533a0
- [9] D. Moncada et al., “Induction of long-term memory by exposure to novelty requires protein synthesis: Evidence for a behavioral tagging,” *Journal of Neuroscience*, vol. 27, no. 28, pp. 7476–7481, 2007. DOI: 10.1523/JNEUROSCI.1083-07.2007
- [10] D. Moncada et al., “Behavioral tagging: A translation of the synaptic tagging and capture hypothesis,” *Neural Plast*, vol. 2015, p. 650780, 2015. DOI: 10.1155/2015/650780
- [11] C. Clopath et al., “Tag-trigger-consolidation: A model of early and late long-term-potentiation and depression,” *PLoS Computational Biology*, vol. 4, no. 12, 2008. DOI: 10.1371/journal.pcbi.1000248
- [12] L. Ziegler et al., “Synaptic consolidation: From synapses to behavioral modeling,” *Journal of Neuroscience*, vol. 35, no. 3, pp. 1319–1334, 2015. DOI: 10.1523/JNEUROSCI.3989-14.2015
- [13] J. Luboeinski et al., “Memory consolidation and improvement by synaptic tagging and capture in recurrent neural networks,” *Commun. Biol.*, vol. 4, no. 1, pp. 1–17, Mar. 2021. DOI: 10.1038/s42003-021-01778-y
- [14] R. Brette et al., “Adaptive exponential integrate-and-fire model as an effective description of neuronal activity,” *J. Neurophysiol.*, vol. 94, pp. 3637–3642, 2005. DOI: 10.1152/jn.00686.2005
- [15] S. Billaudelle et al., “An accurate and flexible analog emulation of AdEx neuron dynamics in silicon,” in *ICECS, 2022*, pp. 1–4. DOI: 10.1109/ICECS202256217.2022.9971058
- [16] M. Hock et al., “An analog dynamic memory array for neuromorphic hardware,” in *Circuit Theory and Design (ECCTD), 2013 European Conference on*, Sep. 2013, pp. 1–4. DOI: 10.1109/ECCTD.2013.6662229
- [17] PowerISA, “PowerISA version 2.06 revision b,” Power.org, Specification, Jul. 2010.
- [18] C. Pehle et al., “The BrainScaleS-2 accelerated neuromorphic system with hybrid plasticity,” *Front. Neurosci.*, vol. 16, 2022. DOI: 10.3389/fnins.2022.795876
- [19] E. Müller et al., “A scalable approach to modeling on accelerated neuromorphic hardware,” *Front. Neurosci.*, vol. 16, 2022. DOI: 10.3389/fnins.2022.884128
- [20] K. Okuda et al., “Initial memory consolidation and the synaptic tagging and capture hypothesis,” *European Journal of Neuroscience*, vol. 54, no. 8, pp. 6826–6849, 2021. DOI: 10.1111/ejn.14902
- [21] A. Prodan et al., “Synaptic tagging and capture: Functional implications and molecular mechanisms,” in *Synaptic Tagging and Capture: From Synapses to Behavior*, S. Sajikumar et al., Eds., 2nd, Cham, Switzerland: Springer, 2024, ch. 1, pp. 1–41. DOI: 10.1007/978-3-031-54864-2\_1
- [22] W. M. Kahan, *IEEE standard 754 for binary floating-point arithmetic*, Lecture Notes on the Status of IEEE, 1996.
- [23] M. Hopkins et al., “Stochastic rounding and reduced-precision fixed-point arithmetic for solving neural ordinary differential equations,” *Phil. Trans. R. Soc. A*, vol. 378, no. 2166, p. 20190052, 2020. DOI: 10.1098/rsta.2019.0052
- [24] W. Dietz et al., “Understanding integer overflow in C/C++,” *ACM Trans. Softw. Eng. Methodol.*, vol. 25, no. 1, pp. 1–29, Dec. 2015. DOI: 10.1145/2743019
- [25] X. Wang et al., “Towards optimization-safe systems: Analyzing the impact of undefined behavior,” in *Proceedings of the Twenty-Fourth ACM Symposium on Operating Systems Principles*, ser. SOSP ’13, Farmington, Pennsylvania: Association for Computing Machinery, 2013, pp. 260–275. DOI: 10.1145/2517349.2522728
- [26] G. E. Forsythe, “Round-off errors in numerical integration on automatic machinery-preliminary report,” *Bull. Amer. Math. Soc.*, vol. 56, pp. 61–62, 1950.
- [27] M. Croci et al., “Stochastic rounding: Implementation, error analysis and applications,” *R. Soc. Open Sci.*, vol. 9, no. 3, p. 211631, 2022. DOI: 10.1098/rsos.211631
- [28] G. Marsaglia, “Xorshift RNGs,” *Journal of Statistical software*, vol. 8, no. 14, pp. 1–6, 2003. DOI: 10.18637/jss.v008.i14
- [29] S. Billaudelle et al., “Structural plasticity on an accelerated analog neuromorphic hardware system,” *Neural networks: the official journal of the International Neural Network Society*, vol. 133, pp. 11–20, Jan. 2021. DOI: 10.1016/j.neunet.2020.09.024
- [30] B. Cramer et al., “Surrogate gradients for analog neuromorphic computing,” *Proc. Natl. Acad. Sci.*, vol. 119, no. 4, 2022. DOI: 10.1073/pnas.2109194119